Scale-model testing of reinforced concrete under impact loading conditions

J. A. SATO
Civil Research Department, Ontario Hydro, 800 Kipling Avenue, Toronto, Ont., Canada M8Z 5S4
F. J. VECCHIO
Department of Civil Engineering, University of Toronto, 35 St. George Street, Toronto, Ont., Canada M5S 1A4
AND
H. M. ANDRE
Civil Research Department, Ontario Hydro, 800 Kipling Avenue, Toronto, Ont., Canada M8Z 5S4

Received November 12, 1987
Revised manuscript accepted February 22, 1989

Aspects of scaling theory relating to the response of reinforced concrete structures under impact load conditions are reviewed. Details for modelling concrete and reinforcement, to be consistent with similitude requirements, are also discussed. A test program is described in which models of varying size were constructed, drop tested, and compared with prototype response. An analysis of the test data is made, indicating that, within certain limitations, the predictions of scaling theory are applicable to reinforced concrete subjected to extreme impact loads.

Key words: cracking, impact, loads, modelling, reinforced concrete, scaling, stresses, structures, tests.

Des aspects de la théorie des modèles à l'échelle reliée au comportement de structures en béton armé soumises à des conditions de charge sont examinés. Les détails de la modélisation du béton et des armatures, afin de respecter les exigences de similitude, sont discutés. Un programme d'essai est décrit dans lequel des modèles de dimensions diverses ont été construits, soumis à des impacts et comparés au comportement du prototype. Une analyse des données d'essai est effectuée; elle indique que les prévisions de la théorie des modèles à l'échelle est applicable, dans une certaine mesure, au béton armé soumis à des charges d'impact extrèmes.

Mots clés: fissuration, impact, charges, modélisation, béton armé, théorie des modèles à l'échelle, contraintes, structures, essais.

[Traduit par la revue]

Can. J. Civ. Eng. **16**, 459–466 (1989)

Introduction

The testing of scale models to study the behaviour of reinforced concrete elements is common practice since the testing requirements of a full-scale model are, in most instances, unmanageable and prohibitively expensive. While scale-related effects can alter the perceived response to some degree, these effects often can be adequately accounted for in most static or dynamic load situations (Andre and Sato 1986). However, less is known about the influence of scale-related effects under extreme impact (i.e., drop) load conditions.

The possible use of reinforced concrete casks for the dry storage, transportation, and final disposal of irradiated nuclear reactor fuel has been under investigation for some time. In 1983, a half-scale model of a potential prototype was constructed and tested by Ontario Hydro (Sato and Vecchio 1985). The model was subjected to two drop tests and a fire test, as would be required by International Atomic Energy Agency (IAEA) regulations for licensing of a prototype container. While the testing of this model was successful, questions arose regarding the validity of using scale models to predict full-scale prototype behaviour under such extreme impact conditions. In response to these concerns, a review of the literature was made and an experimental investigation undertaken. The details and findings of these investigations are presented in this paper.

Theoretical scaling requirements

Two important aspects of model construction and response analysis are the requirements of geometric similitude and materials similitude. Both must be satisfied in order for a proper model to exist.

Geometric similitude requires that all linear dimensions of both the specimen and the load application system be scaled down from the corresponding dimensions of the prototype by a constant ratio, $1/S_l$, where S_l is the scale factor. Materials similitude requires that, at any given load, the stress and strain in the model and prototype must be related by a constant stress factor, S_s, and a constant strain factor, S_e. In principle, this requirement allows for different materials to be used in the model and prototype, but is typically applicable only to modelling elastic response.

In the case of modelling extreme nonlinear dynamic behaviour, as in reinforced concrete under impact loads, the technique of replica scaling is often employed (Barr *et al.* 1980; Davies 1980). Replica scaling requires that all models be exact geometric replicas of the prototype, and that the material behaviour of the model and prototype be identical (i.e., $S_s = S_e = 1.0$) (McHugh *et al.* 1981). Further, if these two conditions of replica scaling are satisfied, then scaled relationships between various aspects of the model and prototype geometry and response can be calculated. These relationships are presented in Table 1 (McHugh *et al.* 1981).

Two relationships in Table 1 are of note. First, it is indicated that the velocity of the model and prototype must be identical. In drop tests where the model and prototype are stationary when released from the same height, this relationship is usually satisfied. Second, Table 1 indicates that the gravitational acceleration must be scaled. For drop tests, this requirement is neglected since the acceleration due to impact is usually considerably greater than the gravitational acceleration (McGovern and Thunborg 1971; Krawinkler and Moncarz 1982). In

NOTE: Written discussion of this paper is welcomed and will be received by the Editor until December 31, 1989 (address inside front cover).

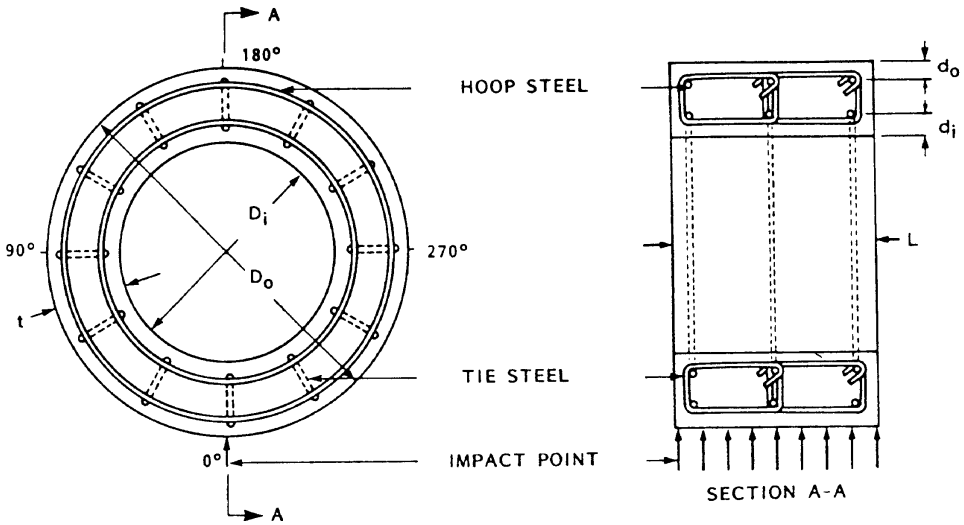

FIG. 1. Specimen shape and reinforcement details.

TABLE 1. Scaling of variables

Variables	Prototype	Model
Length	L	L/S_l
Displacement	x	x/s_l
Strain	ε	ε
Stress	σ	σ
Force	F	F/S_l^2
Time*	T	T/s_l
Strain rate	$\dot{\varepsilon}$	$\dot{\varepsilon}S_l$
Velocity	V	V
Energy	e	e/S_l^3
Acceleration	a	aS_l
Gravitational acceleration	g	gS_l
Density	ρ	ρ
Mass	M	M/S_l^3
Elastic modulus	E	E

NOTE: S_l = scale factor ≥ 1.
*Any characteristic time of the material.

situations where the dead load component is not neglible, the requirement of scaling gravity can be accounted for by adjusting the mass of the models.

Replica scaling in reinforced concrete is especially difficult because of the requirement that both the steel and the concrete be modelled exactly. Aspects of concrete behaviour which must be precisely matched include compressive stress–strain behaviour, tensile stress–strain behaviour, bond between reinforcement and concrete, and aggregate interlock at a crack interface. To preserve the bond and aggregate interlock characteristics between the prototype and the scale model, the maximum aggregate size must be scaled. Scaling of the maximum aggregate size has been found to have negligible effect on the compreseive strength (McHugh *et al.* 1981), but its effect on the tensile strength has not been established.

Correct modelling of the reinforcing steel is also critical. The steel for the model and the reinforcement should be identical in terms of yield strength, ultimate strength, elastic modulus, and strain hardening. In addition, the nature of the surface deformations must be duplicated in order to properly simulate the bond characteristics. Placing and detailing patterns must also be consistent.

Test program

The test program involved drop testing four thick-walled cylinder specimens of various size (see Fig. 1). Simplicity in the design of the specimens was desired to facilitate construction of replica models, and to not further complicate structural behaviour and analysis of test data.

The largest of the four specimens, Model 1, had an outside diameter of 1000 mm and was considered the full-scale prototype. Models 2, 3, and 4 were scale models of the prototype and had outside diameters of 825, 575, and 250 mm, respectively. Complete as-built dimensions are given in Table 2. Although great care was taken in assembling the models, problems associated with tolerances of the bent reinforcing steel meant that some small differences existed in the scaling factors for various aspects of the model geometry. An overall average scale factor, S_l, for each model is given in Table 2.

The concrete used for the models was of normal weight with a target strength of between 40 and 45 MPa. For each model, the concrete was hand batched with proper allowances made for aggregate scaling. (Mix proportions and batching and casting procedures are discussed elsewhere (Andre and Sato 1986).) Given in Table 3 are the material properties for the concrete of each model. The compressive strength, split-tensile strength, and elastic modulus were determined from tests based on ASTM standards C 39, C 496, and C 469, respectively. The variations in these measured properties were within $\pm 5\%$ of mean values, and thus the replica scaling requirement of identical material behaviour was considered as being achieved.

The circumferential reinforcement for models 1 through 4 was fabricated from reinforcement bar types 20M, 15M, 10M, and D3 (Stelco designation), respectively. Tie reinforcement was constructed from 10M, D10, and D5 bars and 3 mm diameter smooth wire, respectively. The steel material properties, as determined using ASTM standard A 370, are also given in Table 3. The circumferential reinforcement bars used for the four models showed very similar properties in the important aspects of response such as yield strength, yield strain, modulus of elasticity, and strain at onset of strain hardening. The tie reinforcement showed more scatter. However, the drop test results (to be discussed) revealed that little to no cracking occurred across the ties and thus the variation in their properties is not significant.

TABLE 2. As-built specimen dimensions

Model No.	D_o (mm)	D_i (mm)	t (mm)	L (mm)	Hoop steel Type	Hoop steel ϕ (mm)	Hoop steel d_o (mm)	Hoop steel d_i (mm)	Tie steel Type	Tie steel ϕ (mm)	M (kg)	Average scale factor (S_f)
1	1000	600	199	529	20M	19.5	63	61	10M	11.3	695.8	1
2	825	495	165	430	15M	16.0	47	55	D10	9.0	377.8	1.23
3	575	345	116	305	10M	11.3	31	30	D5	6.4	128.8	1.79
4	250	153	49	135	D3	4.95	14	15	Wire	3.0	10.9	4.02

TABLE 3. Material test results

Model No.	Concrete f'_c (MPa)	Concrete f_t (MPa)	Concrete ε_0 (MPa)	Concrete E_c (MPa)	Reinforcing steel A_s (mm^2)	Reinforcing steel f_y (MPa)	Reinforcing steel f_u (MPa)	Reinforcing steel E_s (MPa)
1	44.8	4.4	0.0016	55 250	300	440	713	176 000
2	46.5	4.0	0.0016	56 750	200	431	644	179 580
3	42.4	4.5	0.0019	48 421	100	450	681	180 000
4	42.4	4.5	0.0019	48 421	19.2	521	756	186 070

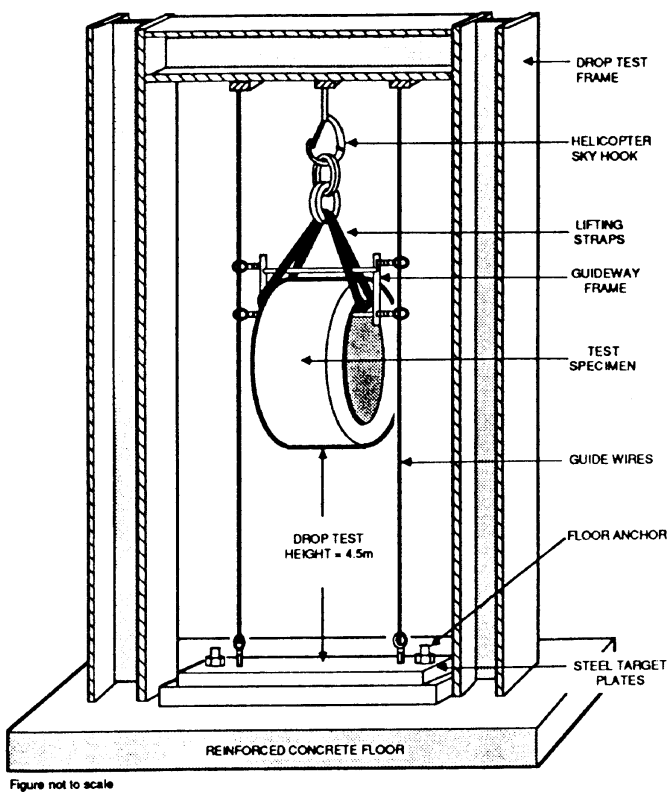

FIG. 2. Schematic representation of test setup.

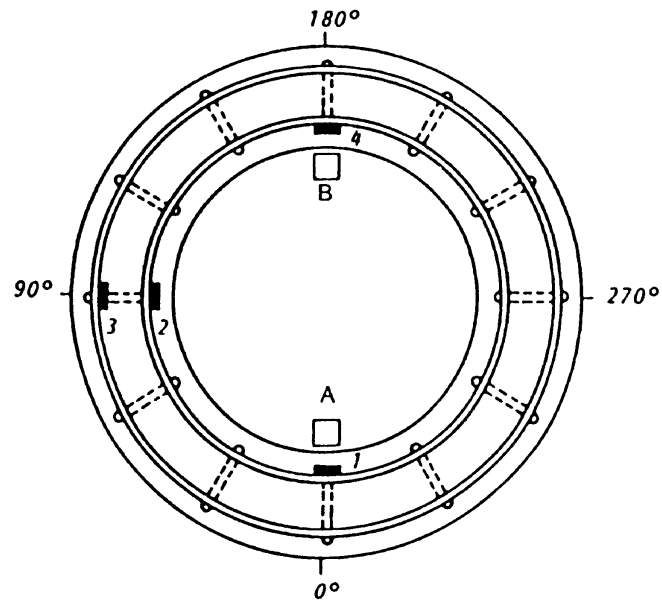

FIG. 3. Instrumentation of test specimens: □, accelerometers; ■, strain gauges. (Notes: (a) strain gauges 1 and 4 only for Model 4; (b) accelerometer A only for models 3 and 4.)

The testing procedure consisted of dropping the specimens from a height of 4.5 m onto a 600 mm thick, heavily reinforced concrete floor. The surface of the floor was armoured with two steel plates, 400 mm in total thickness, that were post-tensioned to the floor. The bolting of the steel plates to the floor was to insure that this combined system would provide enough inertial resistance to adequately simulate an unyielding target for all models. The models were released from a hoist using an electronically controlled sky hook. Their fall was controlled by a guide system consisting of steel cables and eyebolts. A schematic illustration of the test setup is given in Fig. 2.

The models were instrumented with accelerometers and strain gauges (see Fig. 3), configured for high-speed data acquisition using an FM tape recorder. The accelerometers were typically located at 0 and 180°C, relative to the impact point meridian, on the inside surface of the model and at the midpoint of its length. The strain gauges were applied to the circumferential reinforcement bars at the mid-length of the test cylinder. The types of strain gauges and adhesives used were selected such as to minimize time lag effects between the steel deformation and the strain gauge deformation. High-speed photography (1000 frames/s) was used to record the specimen behaviour including

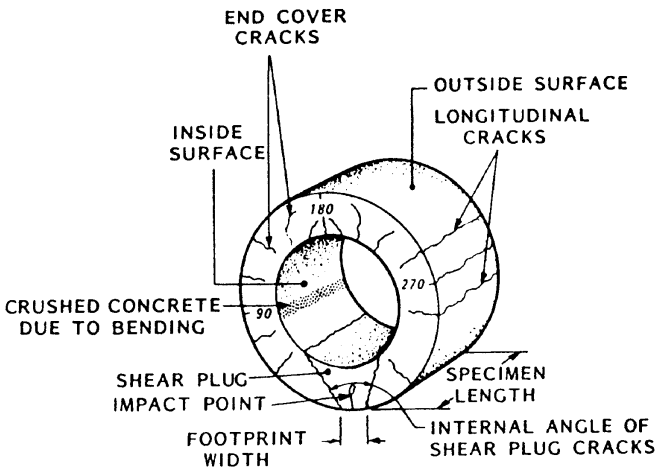

FIG. 4. Typical damage patterns.

crack formation and propogation, and deformations, that occurred during impact.

Test observations

The typical damage patterns observed in the models are shown in Fig. 4. Model 1, considered the prototype specimen, sustained a flat impact onto the steel plates (i.e., without pitch), registering a peak deceleration of 5775 g. The location of the 0°C meridian relative to the impact footprint, however, indicated that the specimen rolled approximately 3° prior to impact. The specimen bounced once after impact to a height of 95 mm, but did not sustain additional damage. The high-speed film revealed that the chronological occurence of damage was as follows: (*i*) shear plug cracks formed, originating from the impact point with an internal angle of 81°; (*ii*) the shear plug was pushed inward, and longitudinal cracks formed on the surface in the area of the 90 and 270° meridians; (*iii*) concrete crushed on the inside surfaces at the 90 and 270° meridians; and (*iv*) the end cover began to spall off. Approximately 65% at the concrete cover spalled or was loose, with fracture occurring through the cement paste, through the aggregates, and at the aggregate–cement interface.

Model 2 experienced a flat impact on the steel plates, with no visible rotation observed, and bounced once after impact to a height of about 120 mm. The deceleration experienced at the 0° meridian was beyond the useable range of the particular accelerometer used at that location. Based on the recorded response prior to saturation, the peak deceleration was estimated to be 6150 *g*. The sequence of damage was identical to that observed with Model 1. The extent of spalling was less, however, with approximately 40% of the cover concrete coming loose.

Model 3 did not impact squarely onto the steel plates, confirmed both by the high-speed films and the impact footprint. The resulting double impact, as first one end hit and then the other, produced a lower than expected peak deceleration of 4794 *g* and also influenced the damage patterns. The model bounced twice, with the first to a height of 150 mm and the second much smaller. Again, the sequence of resulting damage was similar to that experienced by the first two models, with the only notable difference being in the degree of spalling. Model 3 had about a 10% cover loss at the front end and 20% cover loss at the back, the disparity arising from nonuniform initial impact. The spalled surface had considerably less aggregate–cement interface failure than did Model 1, resulting in a smoother fracture surface.

Model 4 experienced a flat impact, but with a 2° roll prior to impacting. A peak deceleration of 17 340 *g* was registered. The model bounced once to a height of 70 mm. Again the sequence of damage was similar to the others except that the shear cracks formed at a more obtuse angle of 86°, and that the shear plug was not pushed inward to any great extent. This smallest model experienced very little end cover loss, at less than 5% for both front and back.

Generally, the models exhibited similar damage patterns, although the amount of surface damage experienced increased with the size of the specimen. Figure 5 shows each model after impact.

The decelerations measured at the impact location (i.e., at 0° meridian) were highest for the smallest scale specimen (Model 4), and relatively low and uniform for the other three models (see Table 4). Also note that the deceleration measured at the 180° meridians for models 1 and 2 were smaller than those recorded at the 0° meridan by nearly an order of magnitude. This is an indication of the high amount of energy absorbed in the specimen deformations.

Strain rates, recorded during the drop tests at instrumented rebar locations, are also summarized in Table 4. The measured strain rates generally tended to increase with the scale factor. (The maximum recorded reinforcement strains, on the other hand, were fairly uniform at 2–3 times the yield strain of the steel.)

The deformation response of the models were compared in terms of maximum ovalling, permanent ovalling, and footprint width (see Table 4). The maximum ovalling was determined from the high-speed films and was defined as the maximum change in the absolute inside surface diameters. The permanent ovalling was taken as the nonrecoverable deformation of the inside diameter, measured after the drop. The fooprint width was defined as the width of the impact zone flattened due to the force of the impact. As can be seen in Table 4, the deformations observed generally increased with the scale factor.

Observations were also made with respect to crack widths and crack spacings (Table 4). (Note: The localized crack conditions refer to the conditions in the most heavily cracked regions.) In most respects, cracking was severest in the large-scale specimens.

Analysis of test results

Scaling theory suggests that the failure patterns and extent of damage should be identical for the four models. The failure modes were, in fact, similar with all four models experiencing the formation of a shear plug at the impact point with an internal angle of about 80°, crushing of the concrete on the inner surface at 80 and 280° meridians, flexural cracking on the outer surface at 30–120° and 240–330°, and cracking on the inner and outer surfaces at 180°. However, there were significant differences in the extent of damage sustained by the models. In particular, the amount of end cover spalling decreased dramatically with decreasing model size. Contributing factors to this irregularity may include the difficulty in modelling the micro aspects of concrete which govern fracture toughness (Carpinteri 1982), the very high strain rates observed in the smaller models resulting in higher tensile strength (Suaris and Shah 1983), and lower-than-expected deceleration forces in the smaller models. There was also noticeable decrease in the extent of concrete crushing damage sustained by the smaller models. This may, in part, be

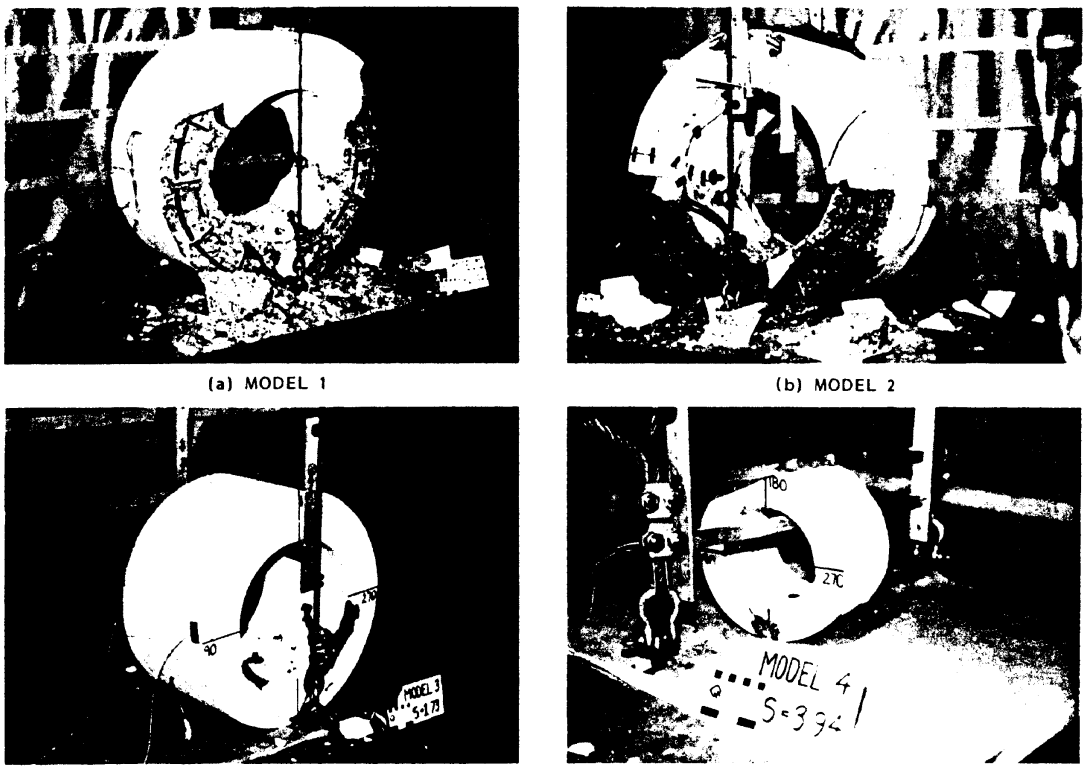

FIG. 5. Photographs of models after drop testing.

TABLE 4. Test results

(a) *Instrument data*

Model No.	Peak deceleration (g) 0°	Peak deceleration (g) 180°	Duration of peak ($X10^{-6}$ s)	Strain rate ($mm \cdot mm^{-1} \cdot s^{-1}$) SG 1	SG 2	SG 3	SG 4
1	5 775	615	345	6.448	—	5.650	11.306
2	6 150	691	286	5.580	2.070	9.080	14.372
3	4 794	—	448	11.160	2.575	12.107	15.027
4	17 339	—	126	20.726	—	—	19.908

(b) *Deformations*

Model No.	Permanent ovalling Horizontal (mm)	% change	Vertical (mm)	% change	Maximum ovalling Horizontal (mm)	% change	Vertical (mm)	% change	Footprint width (mm)
1	620	+3.3	588	−2.0	641	+6.8	557	−7.2	150
2	510	+3.0	485	−2.0	522	+5.5	465	−6.1	103
3	355	+2.9	338	−2.0	354	+2.6	333	−3.5	82
4	156	+2.0	150	−2.0	161	+5.2	144	−5.9	27

(c) *Cracking*

Model No.	Outside surface Avg. crack width (mm)	Outside surface Avg. crack spacing (mm)	Inside surface Avg. crack width (mm)	Inside surface Avg. crack spacing (mm)	Maximum crack width (mm)	Avg. width of widest crack (mm)
1	0.66	170	0.65	299	3.0	2.5
2	0.55	139	0.52	179	2.5	1.5
3	0.38	126	0.29	162	1.5	1.3
4	0.22	65	0.21	52	0.9	0.8

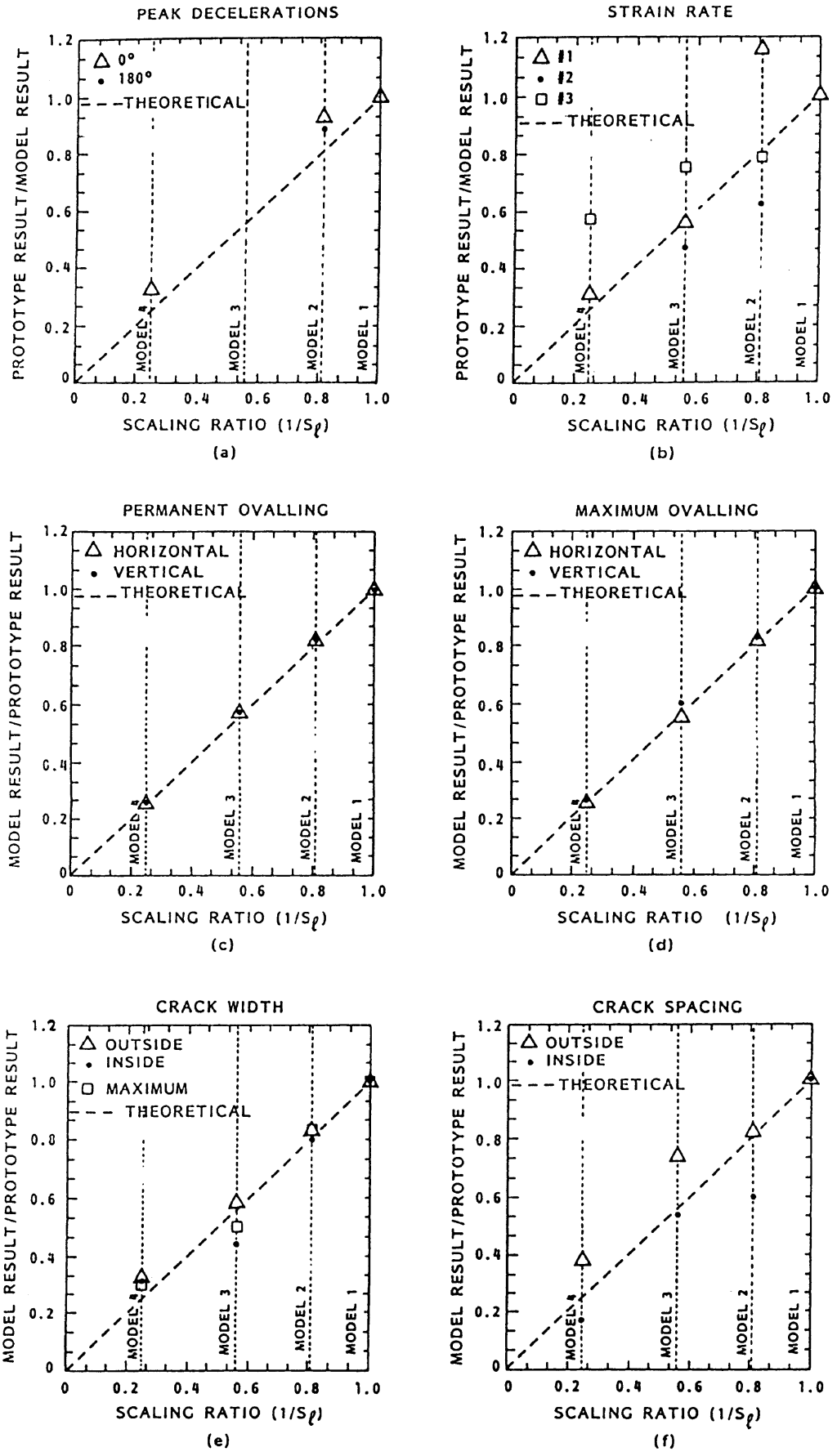

FIG. 6. Comparison of test results with theoretically predicted response.

explained by increases in concrete compressive strength due to strain-rate effects (Ahmad and Shah 1985). Enhancement of the reinforcement steel properties in the smaller models, again as a result of strain-rate effects (Mainstone 1975), may also have been a contributing factor.

Based on the scaling laws, the peak decelerations should vary in direct linear proportion to the scale factor. The duration of the deceleration event, on the other hand, should vary inversely with the scale factor. A comparison of the observed deceleration data with the scaling laws is presented in Fig. 6*a*, showing the peak decelerations recorded at 0° and 180°. Except for the results of Model 3, which sustained a double impact, the experimental values are seen to be in reasonable agreement with the results predicted by scaling theory. Similar agreement was seen in the deceleration duration data.

The straining rates in the constituent materials of a model are, according to scaling laws, also related linearly. A comparison of the observed strain rates with the values predicted by theory is given in Fig. 6*b* for various gauge locations on the reinforcement. While significant scatter exists in the results, the general trend is consistent with scaling theory. The large scatter is largely attributable to the random proximity of the gauges to cracks forming in the specimens. A strain gauge located directly at a crack surface would experience a much more rapid increase in strain than would a gauge located between cracks.

Data pertaining to deformation can be analyzed by two different means: (*i*) by examining the percentage change from the undeformed to the deformed state; or (*ii*) by comparing the absolute dimensions of the deformed specimens. The percentage change values can be considered as a strain and thus, according the the scaling laws, should be the same for all models. The absolute dimensions of the deformed specimens, on the other hand, are predicted to be inversely proportional to the scale factor. The percentage changes in the dimensions of the model are included in Table 4. Good agreement with theory is seen with respect to permanent ovalling, in both the horizontal and the vertical direction, where values of +3.0 and −2.0%, respectively, were typically measured. The maximum ovalling percentage change values, estimated from high-speed films, were not as consistent. In terms of absolute deformations, comparisons of permanent ovalling and maximum ovalling are made in Figs. 6*c* and 6*d*, respectively. Excellent agreement is obtained in all respects.

The footprint width is another permanent deformation which should be in inverse proportion to the scale factor. A comparison of the experimental results with the theory shows reasonable agreement. In all cases, however, the footprint width is underpredicted by the models. This is possibly the result of an increase in the compressive strength of the concrete in the smaller models due to strain-rate effects.

Crack widths are absolute deformations related to the strain of a specimen. As such, scaling theory suggests that crack widths in a model should relate to crack widths in the prototype in inverse proportion to the scale factor. Given this, it follows that the crack spacing must also be scaled by the same factor in order for the requirement of identical strain in all models to be satisfied. Figure 6*e* compares the average crack widths, determined from crack mappings, with theoretically predicted values. Reasonably good accuracy is obtained, with Model 4 results overpredicting crack widths in the prototype, while models 2 and 3 results underpredicting prototype crack widths. Figure 6*f* presents average crack spacing results compared with theoretical trends. A larger scatter of these results is seen. Generally, the outside surface crack spacing for the models is overpredicted, meaning fewer more widely spaced cracks. The inside surface crack is generally underpredicted, meaning that the smaller models were more severely cracked. The fact that these two results show opposite behaviour indicate that while crack data may be in general agreement with scaling theory, behaviour is susceptible to wide variations brought on by the natural randomness of concrete cracking. Similar patterns were observed when examining maximum crack width and average width of the widest crack.

Conclusions

The experimental results obtained indicate that reinforced concrete sacle models, when fabricated and tested to the requirements of replica scaling, can be used to accurately predict many aspects of prototype behaviour under impact loading conditions. Damage patterns, specimen deformations, and average crack conditions were visible characteristics which followed the patterns predicted by scaling laws. Other aspects of response measured, and found to also generally follow theoretically predicted response, included peak decelerations, durations of peak deceleration, strain rates, and local crack patterns. However, due to the limited number of data and scatter of some of the results, additional data from further testing is warranted to confirm the suggested compliance with theory.

The test results also served to reinforce the knowledge that a high degree of randomness is involved in impact load conditions (e.g., orientation at impact) and in material behaviour (e.g., concrete cracking). Thus, a scale-model study of prototype behaviour should necessarily involve several specimens to obtain a good statistical indication of response. Further, more accurate results are obtained from larger scale specimens due to the reduced influence of strain-rate effects on concrete tensile strength and compressive strength.

Acknowledgements

The experimental program reported in this paper was funded by, and conducted at the facilities of, Ontario Hydro. The authors wish to express their sincerest appreciation for the support received.

AHMAN, S. H., and SHAH, S. P. 1985. Behaviour of hoop confined concrete under high strain rates. American Concrete Institute Journal, **82**(5): 634–647.

ANDRE, H. M., and SATO, J. A. 1986. Modelling reinforced concrete for impact loading: phase I. Report No. 86–216–K, Ontario Hydro Research Division, Toronto, Ont.

BARR, P., BROWN, M. L., CARTER, P.G., HOWE, W. D., JOWETT, J., NEILSON, A., and YOUNG, R. L. D. 1980. Studies of missile impact with reinforced concrete structures. Nuclear Energy, **19**(3): 179–189.

CARPINTERI, A. 1982. Application of fracture mechanics to concrete structures. ASCE Journal of the Structural Division, **108**(4): 833–848.

DAVIES, I. L. 1980. Damaging effects from the impact of missiles against reinforced concrete structures. Nuclear Energy, **19**(3): 199–205.

KRAWINKLER, H., and MONCARZ, P. D. 1982. Similitude requirements for dynamic models. *In* Dynamic modelling of concrete structures. Publication SP–73, American Concrete Institute, Detroit, MI, pp. 1–22.

MAINSTONE, R. J. 1975. Properties of materials at high rates of straining or loading. The effect of impact loading on building. International Union of Testing and Research Laboratories for Materials and Structures (RILEM) Committee, Paris, France, pp. 102–116.

McGOVERN, D. E., and THUNBORG, S. 1971. On the use of modelling in a structural response problem. Sandia Laboratory, Albuquerque, NM.

McHUGH, S., GUPTA, Y., and SEAMAN, L. 1981. Pipe missile impact experiments on concrete models. Project Report, Electrical Power Research Institute (EPRI), Palo Alto, CA.

SATO, J. A., and VECCHIO, F. J. 1985. Concrete integrated cask program: structural testing of a half scale model. Report No. 85–65–H, Ontario Hydro Research Division, Toronto, Ont.

SUARIS, W., and SHAH, S. P. 1983. Properties of concrete subjected to impact. ASCE Journal of Structural Engineering, **109**(7): 1727–1741.

List of symbols

a	acceleration
A_s	cross-sectional area of reinforcement
d_1	location of inside hoop rebar (see Fig. 1)
d_o	location of outside hoop rebar (see Fig. 1)
D_i	inside diameter of cylindrical test specimen
D_o	outside diameter of cylindrical test specimen
e	energy
E	modulus of elasticity
E_c	modulus of elasticity of concrete (initial stiffness tangent)
E_s	modulus of elasticity of steel
f'_c	concrete compressive strength
f_y	yield stress of reinforcing steel
f_u	ultimate stress of reinforcing steel
F	force
g	gravitational acceleration
L	length of cylindrical test specimen
M	mass
S_e	strain factor
S_l	scale factor (≥ 1.0)
S_s	stress factor
t	thickness of cylinder wall
T	time
V	velocity
x	displacement
ε	strain
ε_y	yield strain
$\dot{\varepsilon}$	strain rate
ϕ	diameter
ρ	density
σ	stress